

Mn-doped FeOOH modified g-C₃N₄ as 3D tubular heterogeneous catalysts for Photo-Fenton removal of organic pollutants

Liumi Deng ^a, Meng Liao ^a, Xuejing Wei ^a, Zixuan Zou ^a, Shaohua Chen ^{a,*}, Hua Wang ^{a,*}, Jiayue Chen ^{b,*}

^a College of Materials Science and Engineering, Hubei Provincial Engineering Research Center of Industrial Fiber Preparation and Application, Wuhan Textile University, Wuhan 430200, Hubei, China

^b Sichuan Silk Engineering Technology Center, Sichuan Academy of Silk Sciences Co., Ltd., Chengdu 610031, People's Republic of China

* Corresponding authors.

Corresponding authors: Shaohua Chen ^{a,*}, Hua Wang ^{a,*}, Jiayue Chen ^{b,*}

Email: shaohuachen@foxmail.com, huawangabc@163.com, cjy9480@139.com.

Text:

Text S1 Reagents and materials

Rhodamine B (RhB, C₂₈H₃₁ClN₂O₃), ferrous sulfate (FeSO₄•7H₂O), Manganese sulfate monohydrate (MnSO₄•H₂O), ammonium bicarbonate (NH₄HCO₃), hydrogen peroxide (H₂O₂, 30 wt %), 5,5-dimethyl-1-pyrroline-N-oxide (DMPO) were obtained from Sinopharm Chemical Reagent Co., Ltd. Melamine (C₃H₆N₆), urea (CH₄N₂O), formic acid (HCOOH), acetonitrile (C₂H₃N) and absolute ethyl alcohol were purchased from Aladdin Chemical Company. All reagents were not further purified. Deionized (DI) water was used in the experiment.

Text S2 Materials characterization and experiments

The crystal phases of the materials were analyzed on Rigaku mini flex 600 X-ray diffraction (XRD, Rigaku Corp., Tokyo, Japan) using Cu K α radiation in the range of 10° to 80° for 5 min. The bonding configurations of the samples were characterized by FT-IR spectroscopy with an FTIR-650 spectrometer ((FT-IR, Sci.&Tech. Development Co. Ltd., Tianjin, China). The surface areas of the materials were characterized using

Brunauer–Emmett–Teller method on a Micromeritics ASAP 2460 (BET, Micromeritics Instrument Corp, USA). The surface morphology and elemental content of the materials were characterized via JSM-IT300A (SEM-EDS, JEOL Co., Ltd., Tokyo, Japan) scanning electron microscopy under an EDS energy spectrum. The chemical elements and elemental forms of the materials were characterized by X-ray photoelectron spectroscopy (XPS, Thermo Scientific K-Alpha, Thermo fisher the USA). The binding energy was calibrated using the C1s level at 284.8 eV as an internal standard. The photoluminescence (PL) spectra of the materials were measured by Hitachi F-7000 spectrometer at 320 nm excitation wavelength. Ultraviolet-visible diffuse reflection spectroscopy was performed in the 200-800 nm range with a Lambda 950 spectrophotometer and the reflection standard was BaSO₄ ((UV-vis DRS, UV-3600Plus, Shimadzu, Japan)). The electron paramagnetic resonance (EPR) spectrum of the hydroxyl radical spin trapped by 5,5-dimethyl pyridine N-oxide (DMPO) was analyzed on Bruker EMXplus-6/1 (Bruker, Germany).

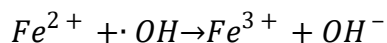
Photoelectrochemical performance: 10 mg of powder sample was dispersed in 1 mL of ultrapure water/ethanol solution, then 50 μ L of Nafion solution was added and sonicated for 30 min to form a homogeneous suspension, then 100 μ L of suspension was added dropwise on ITO glass and dried at room temperature. Transient photocurrent density (*i-t*) and electrochemical impedance spectroscopy (EIS) were conducted using an electrochemical workstation (CHI660E) in 0.5M Na₂SO₄ electrolytes. Three-electrode system (counter electrode: Pt electrode; reference electrode: Ag/AgCl; working electrode: ITO) was used.

Ultra-performance liquid chromatography-high resolution tandem mass spectrometry (UPLC-HRMS/MS, QExactive, ThermoFisher Scientific) was used to determine the intermediates of RhB. The intermediates after RhB degradation were separated by liquid chromatography using Dionex Ultimate 3000 UHPLC on a C-18 column. An isocratic 1% formic acid aqueous/acetonitrile (50:50, v/v) solution was used as the mobile phase at a flow rate of 0.5 mL/min. The sample injection volume was 10 μ L. The mass spectrometer was operated in the range of 50-700 *m/z*. The chromatographic separation was performed on a C-18 column. The capillary

temperature and voltage were maintained at 320 °C and 50 V, respectively, and the spray voltage was 3.8 kV).

Text S3 Effect of initial catalyst dosage

In order to investigate the effect of catalyst dosage on the degradation efficiency, a series of degradation experiments were carried out by varying the catalyst dosage (from 50 mg to 250 mg) while other experimental conditions remained unchanged. As shown in Fig. S7, when the amount of 2Mn-FeOOH/gC₃N₄ was increased from 50 mg to 200 mg, the degradation efficiency of rhodamine B increased from 81% to 97% in 30 min. The increase in the catalyst content and the increase in the active sites could rapidly activate hydrogen peroxide and generate a large number of hydroxyl radicals, thus improving the degradation efficiency. However, when the dose of 2Mn-FeOOH/gC₃N₄ was increased from 200 mg to 250 mg, the degradation efficiency instead showed a decrease, which was due to the elimination of free radicals by Fe²⁺. The excess Fe²⁺ reacted with the generated hydroxyl radicals, resulting in the deactivation of the active site and the elimination of the free radicals, which led to the decrease in the degradation efficiency, as Eq. (S1) shown. So, 200 mg of catalyst was chosen as the optimum dosage for further experiments.



(S1)

Text S4 TOC Removal

Before the TOC test, 5 ml of the reaction solution was collected and immediately filtered through a filter membrane to stop the reaction. Na₂S₂O₃ solution was used to dilute the filtrate to 15 ml to obtain the sample solution to be measured. In Fig. S8, the TOC removal was 14% at 15 min and 70% at 30 min. Because of the large amount of organic intermediates produced during the degradation process, there were inconsistency between the TOC removal and the degradation efficiency of the concentration. The small organic molecules were rapidly mineralized at 30 min, which led to a rapid increase in the TOC removal to near 70%. Therefore, the 2Mn-FeOOH/gC₃N₄ degradation process can effectively mineralize rhodamine B molecules and degrade them to inorganic substances.

Figures:

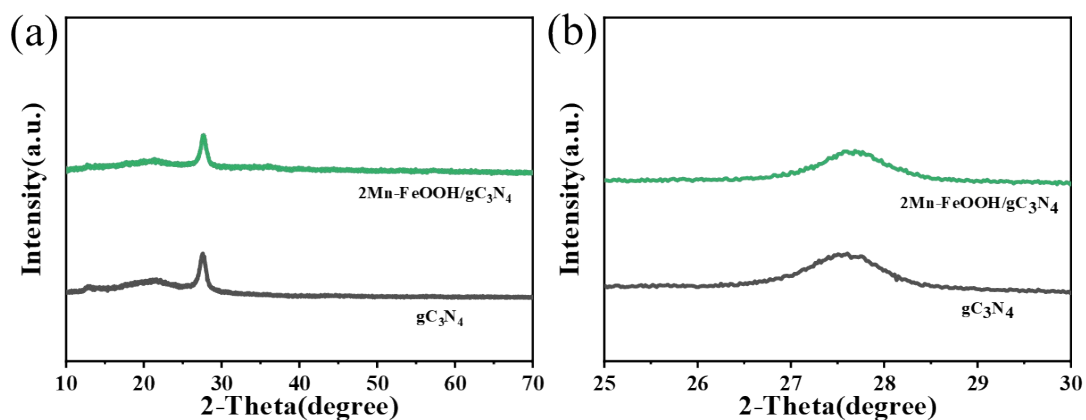


Fig. S1. Magnified XRD patterns at $25^\circ - 30^\circ$ of gC_3N_4 and $2\text{Mn-FeOOH/gC}_3\text{N}_4$.

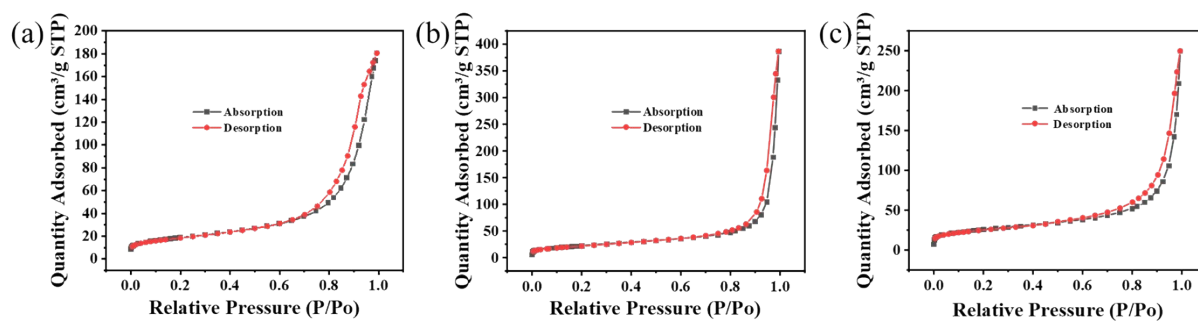


Fig. S2. N_2 adsorption-desorption isotherms of Mn-FeOOH (a), gC_3N_4 (b) and $\text{FeOOH/gC}_3\text{N}_4$ (c).

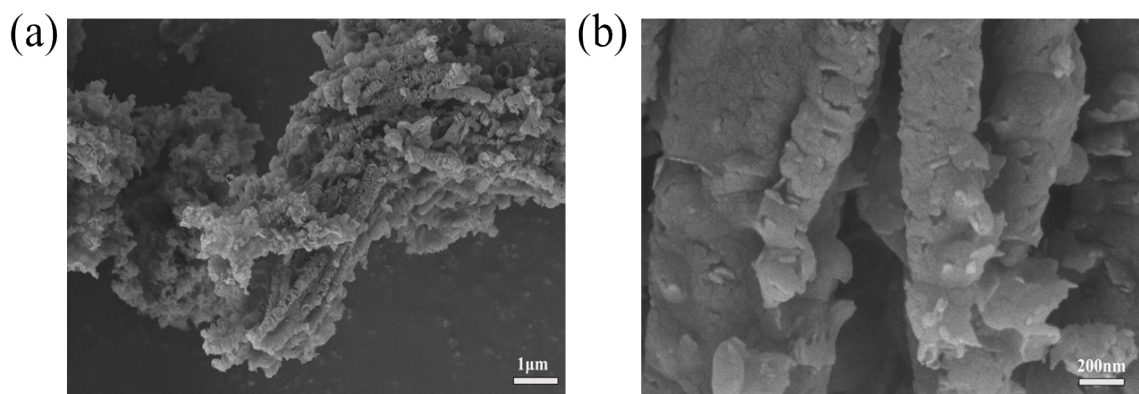


Fig. S3. (a-b) the SEM of gC_3N_4 .

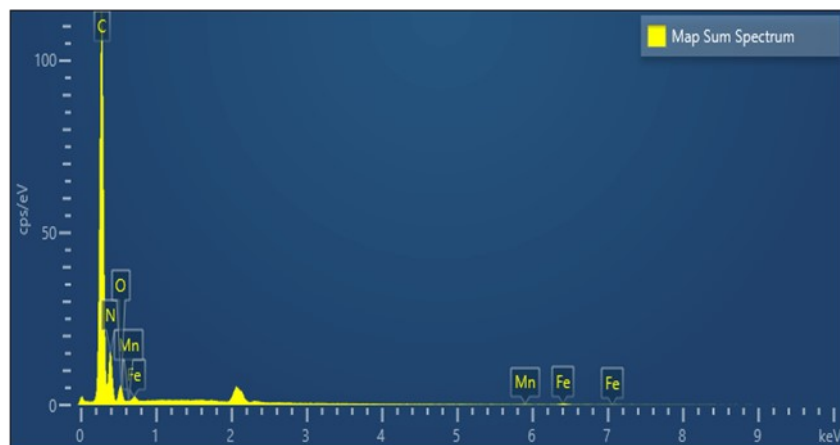


Fig. S4. The elemental analysis of EDS of 2Mn-FeOOH/gC₃N₄ (c).

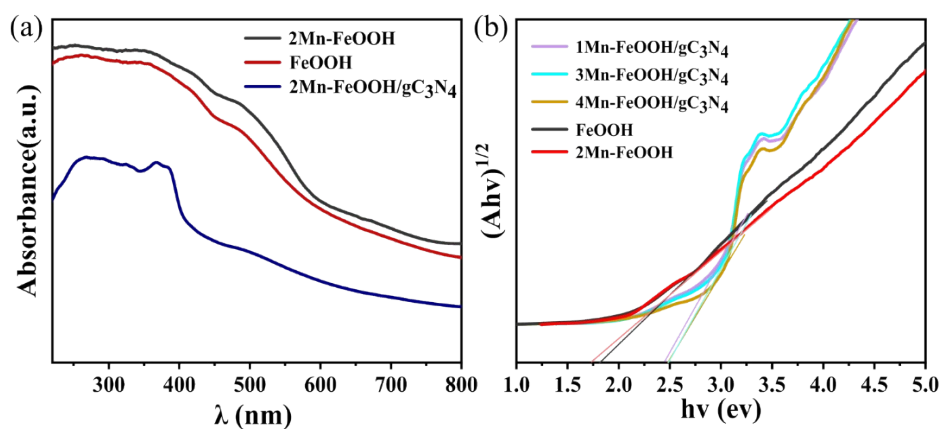


Fig. S5. UV-vis diffuse reflectance spectroscopy spectra (a), and the corresponding calculated band gap of materials

(b).

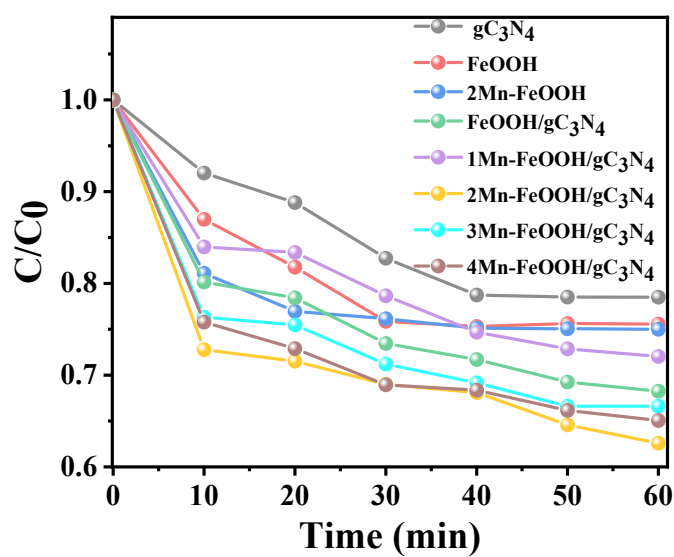


Fig. S6. Adsorption equilibrium of Mn-FeOOH, gC₃N₄ and FeOOH/gC₃N₄ composites.

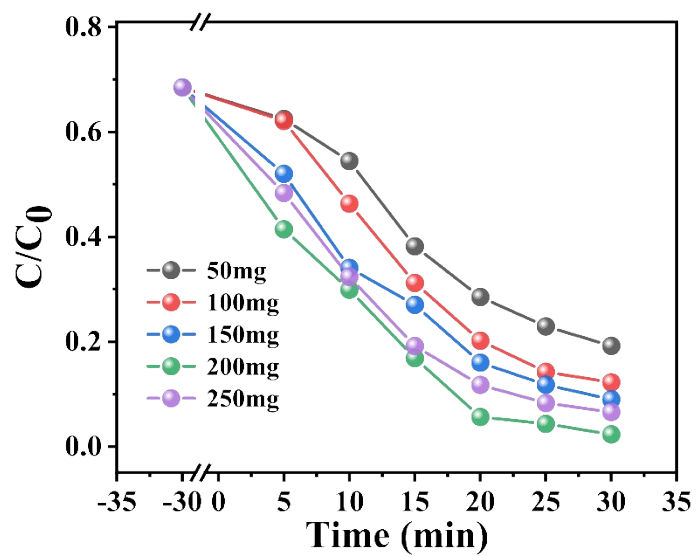


Fig. S7. Effect of catalyst dosage on degradation efficiency of 2Mn-FeOOH/gC₃N₄ on RhB. Experimental condition: T=25 °C, [RhB]=10 mg/L, [H₂O₂]=10 mM.

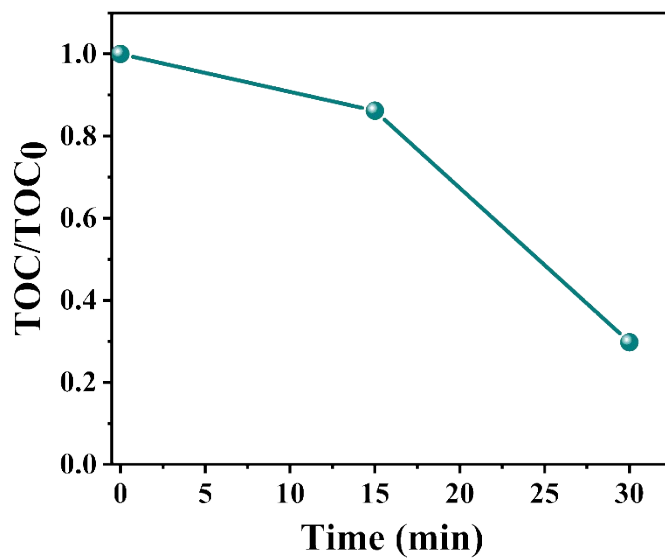


Fig. S8. TOC removal of 2Mn-FeOOH/gC₃N₄ on RhB at 15min and 30min.

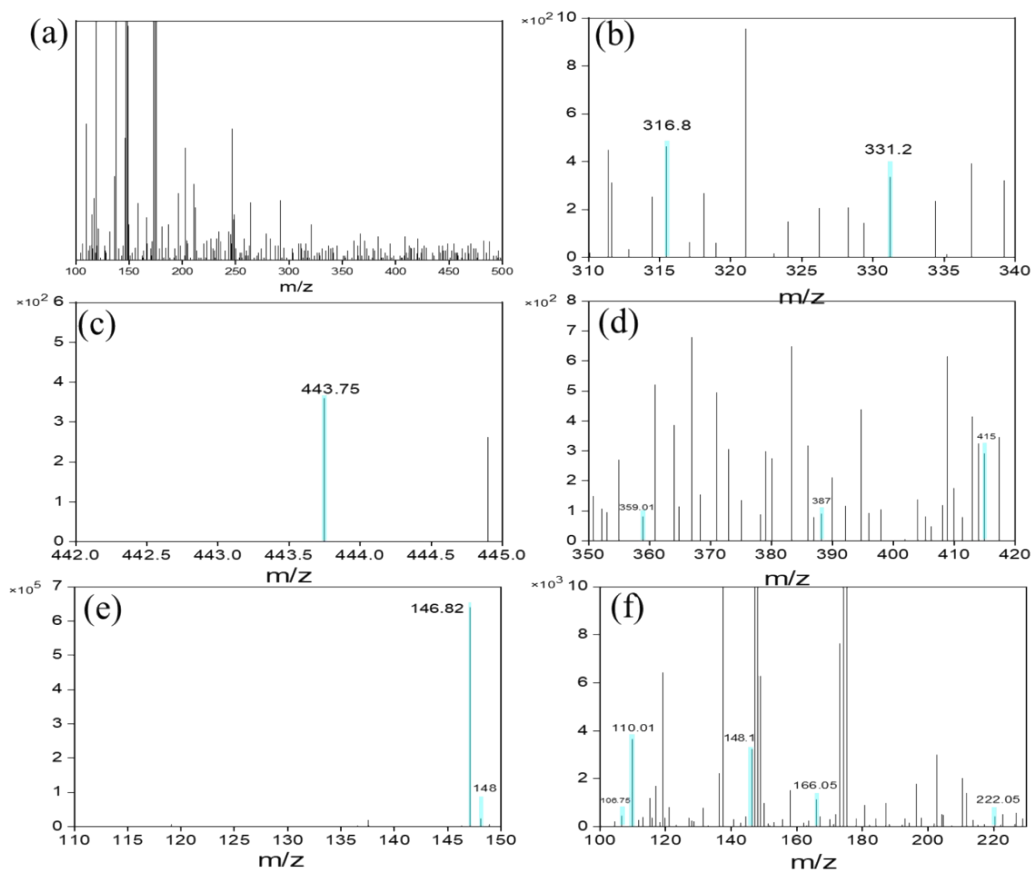


Fig. S9. The intermediates present in the reaction process of LC-MS.

Tables:

Table 1. Physical properties of different samples.

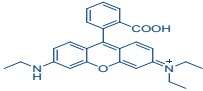
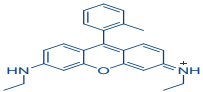
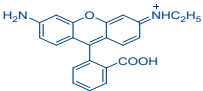
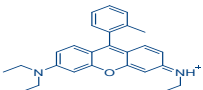
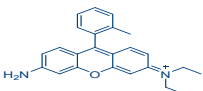
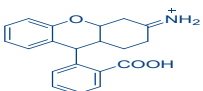
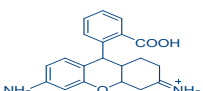
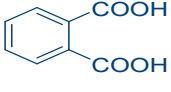
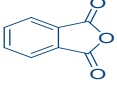
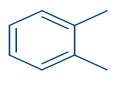
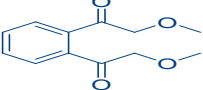
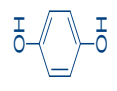

Materials	S_{BET} ($\text{m}^2 \cdot \text{g}^{-1}$)	Pore volume ($\text{cm}^3 \cdot \text{g}^{-1}$) ^a	Pore size(nm) ^b
2Mn-FeOOH	66.2305	0.279195	16.8620
gC_3N_4	81.4569	0.598103	29.3703
FeOOH/ gC_3N_4	91.4184	0.386152	16.8960
2Mn-FeOOH/ gC_3N_4	102.4660	0.433720	16.9313

a :Single point adsorption total pore volume.

b: Adsorption average pore diameter ($4V / S_{\text{BET}}$).

Table 2. The chemical formula of the reaction intermediate.

Number	m/z	Proposed structure
P1	443	
P2	359	

P3	415	
P4	387	
P5	359	
P6	415	
P7	387	
P8	316	
P9	331	
P10	166	
P11	148	
P12	106	
P13	222	
P14	110	
P15	148	
P16	146	